ENHANCEMENT OF CO_2/CH_4 PERMSELECTIVITY VIA THERMAL REARRANGEMENT OF MIXED MATRIX MEMBRANES MADE FROM AN O-HYDROXY POLYAMIDE WITH AN OPTIMAL LOAD OF A POROUS POLYMER NETWORK.

C. Soto[1,2], C. Aguilar Lugo[3,4], S. Rodríguez[1,2], L. Palacio[1,2],

Á.E. Lozano[1,354], P. Prádanos[1,2,], A. Hernandez[1,2,*]*

1. Surfaces and Porous Materials (SMAP), Associated Research Unit to CSIC. University of Valladolid, Facultad de Ciencias, Paseo Belén 7, E-47011 Valladolid, Spain.

2. Institute of Sustainable Processes (ISP), Dr. Mergelina s/n, 47011, Valladolid, Spain.

3. Institute for Polymer Science and Technology (ICTP-CSIC), Juan de la Cierva 3, 28006 Madrid, Spain

4. Instituto de Investigaciones en Materiales, Universidad Nacional Autonoma de Mexico, Ciudad Universitaria, CDMX, 04510, Mexico

5. IU CINQUIMA, University of Valladolid, Paseo Belén 5, E-47011 Valladolid, Spain.

** to whom correspondence should be addressed.*

Abstract

Mixed matrix membranes, MMMs, consisting of variable loads of a porous polymer network, PPN, within an o-hydroxipolyamide, HPA (6FCl-APAF, made from the reaction between 2,2-bis[4-chlorocarbonylphenyl)hexafluoropropane, 6FCl, and 2,2-bis(3-amino-4-hydroxyphenyl)hexafluoropropane, APAF), have been thermally treated to induce the rearrangement of HPA to a polybenzoxazole (β-TR-PBO). HPA is 6FCl-APAF was loaded with a PPN synthetized, by us, by combining triptycene (TRP) and trifluoroacetophenone (TFAP). Mechanical, thermal and morphological properties of the membranes have been determined.

CO_2/CH_4 selectivity of MMMs decreased slightly both when the PPN load was augmented and when thermal rearrangement took place. The changes in selectivity can be attributed mostly to solubility effects for β-TR-MMMs and to diffusive effects for the

MMM from neat HPA. CO_2 and CH_4 permeabilities increased to the 2008 Robeson´s upper bond for an optimal 30 % PPN load both before and after thermal rearrangement. These relatively good permselectivities are explained in terms of compaction, rigidity, fractional free volumes and filling-matrix interactions.

Keywords: Mixed Matrix Membranes; Thermal rearrangement; O-hydroxipolyamide; Polymer Porous Networks; CO_2/CH_4 gas separation.

Introduction

Biogas from the anaerobic digestion (AD) of organic matter or from the gasification-methanation of residual biomass constitutes a renewable energy vector able to reduce fossil fuels consumption and mitigate climate change [1,2] . Today, biogas is mainly produced from the anaerobic digestion of livestock and agro-industrial waste, energy crops, wastewaters or the organic fraction of municipal solid waste [3]. The number of biogas production plants in Europe has increased from 6227 in 2009 up to 17439 by the end of 2016, which has doubled the installed electricity capacity from biogas[4]. Biogas from AD primarily consists of CH_4 (50–70%) and CO_2 (30–50%) [5] and is subjected to the most rigorous quality specifications when used as a substitute of natural gas or as vehicle fuel [6]. The final use of biogas determines the type of upgrading required, which ranges from a conventional H_2S removal for combined heat and power production, to a sequential removal of H_2S, H_2O, CO_2 and other compounds present as methyl-siloxanes when injected into natural gas grids [7]. In this context, upgraded biogas with a CH_4 concentration > 95 % is typically required when injected into the gas grid or compressed and used as transport fuel [8]. For this purpose, CO_2 concentrations must be lowered to 2.5-4 % [9].

Today, a wide range of commercial technologies to remove CO_2 from biogas are available in the market. Physical/chemical methods such as adsorption, absorption, cryogenic and membrane separation are mature technologies that exist at commercial readiness level with upgrading capacities ranging from 100 Nm^3/h to 2000 Nm^3/h [10] [8]. These technologies exhibit a high robustness and efficiency but having high operating cost and environmental impacts as a result of their high energy consumption. On the other hand, biological technologies such as hydrogenotrophic CO_2 reduction to CH_4 using renewable H_2 in archaeal-based bioreactors or microalgae-based CO_2 removal have been

successfully tested at pilot scale and are under validation at semi-industrial scale [11]. Biotechnologies typically exhibit lower operating costs and environmental impacts but require either a close renewable H_2 source or large surface areas and high solar irradiations, conditions that are not ubiquitous in all biogas plants.

In this context, membrane separation has emerged as a promising alternative to conventional CO_2 separation processes due to their high energy efficiency [12], low capital costs and footprint, high robustness, ease of operation and maintenance [13]. Although this technology is already available at commercial scale, there is still need for further research in materials science in order to manufacture membranes with an optimum balance between CO_2 permeability and CO_2/CH_4 selectivity [14]. Indeed, membrane-based CO_2 separation has gained a significant market share from 2012 to 2016 based on the recent advances on polymer science [15]. In this sense, mixed matrix membranes (MMMs) and polymers made by via thermal rearrangement (TR) exhibit a high free volume fraction (FFV) along with a high permeability compared to commercial cellulose acetate [16, 17]. In recent years, a large number of different hypercrosslinked polymers, HCP, or HCP like polymers have been used as fillers to prepare MMMs [18-22]. Metal-Organic Frameworks, MOFs, developed by Khdhayyer et al. [23] seem to reduce physical ageing of mixed matrix material while increasing permeability. Recently, a TR-MMM made of a metal organic framework Porous Aromatic Frameworks, PAF, and a α-TR-PBO (made of o-hydroxypolyimide) showed very good gas separation properties as shown by Kim et al. [24]. Despite the above-mentioned advantages of fillers TR-MMMs, there is room for significant advances by incorporating new fillers as porous polymer networks (PPNs), instead of MOFs, during membrane preparation since PPNs are expected to have high compatibility with the polymeric matrix, and increase permeability when subjected to heat treatment to obtain TR-MMM.

The high CO_2 permeability in TR materials is mediated by the micropores created by the transformation of molecular chains. Recently, a TR-MMM made from a metal organic framework and a α-TR-PBO (made from o-hydroxypolyimide) showed good gas separation properties [24]. Smith et al [25] have used a polymer aromatic framework as a filler (both thermally treated and untreated) to get an α-TR-PBO MMM with very good gas separation properties. As shown by Smith and coworkers, there is room for significant advances by incorporating porous polymer networks (PPNs) within a polymeric matrix able to experiment thermal rearrangement. Here we will use a polymeric matrix containing an o-hydroxypolyamide and a filler consisting in a PPN, with high compatibility with the polymeric matrix and specific interactions with CO_2 induced by its bulky but electron-withdrawing -CF_3 groups. The corresponding MMMs and β-TR-PBO MMMs have been evaluated for their ability to separated CO_2 from CH_4.

In this work, the CO_2 and CH_4 gas permeation properties of MMMs and TR-MMMs have been systematically evaluated. MMMs have been prepared via combination of a poly(hydroxyamide) (HPA, able to undergo a thermal process to TR-PBO) and a PPN. Subsequently, these MMMs have been thermally treated to convert the HPA matrix to polybenzoxazole (β-TR-PBO), thus generating the corresponding TR-MMM, which have been further evaluated for their ability to separated CO_2 from CH_4.

1. Materials and methods

1.1 Reagents and solvents

2,2-bis[4-carboxyphenyl)hexafluoropropane (6F, 98%), 2,2-Bis(3-amino-4-hydroxyphenyl)hexafluoropropane (APAF, 97 %) was purchased from Apollo Scientific (Apollo Scientific, Manchester, United Kingdom). Thionyl chloride ($SOCl_2$, 99.5 %), chlorotrimethylsilane (CTMS, 98 %), pyridine (Py, 99.8 %), N,N-dimethylaminopyridine

(DMAP, 99 %). Anhydrous N,N-dimethylacetamide (DMAc, 99.8 %), N-methyl-2-Pyrrolidinone (NMP, 99.5 %), Tetrahydrofuran (THF, 99.9 %) and chloroform ($CHCl_3$, 99.8 %) were purchased from Sigma-Aldrich (Germany) and were used as received. N,N-dimethylformamide (DMF, 99.8 %) and Dimethylsulphoxide (DMSO, 99.8 %), were purchased from Scharlab (Scharlab, Barcelona, Spain) and were used as received. Methanol (MeOH) reagent-grade quality, from Scharlab too, was used without purification.

1.2 Synthesis of the poly(hydroxyamide)(HPA) 6FCl-APAF as TR precursor

The 6FCl-APAF poly(o-hydroxyamide) has been already synthesized by us [15] but it will be described below because some modifications were introduced.

a) Synthesis of the 6FCl diacid chloride

2,2´-bis(4-chlorocarbonylphenyl)hexafluoropropane diacid chloride (6FCl) was batch-wise prepared according to *Smith et al* [26] in a double neck flask; 13.5 g of 4 4'-(hexafluoroisopropylidene) bis(benzoic acid) (6F) was added and dissolved with 26 mL of $SOCl_2$ under an inert atmosphere (vacuum was applied to the system) and constant agitation, maintaining the reaction at 0 °C before the slow addition of $SOCl_2$. Then, 0,5 mL of DMF was slowly added to prevent secondary reactions mediated by high temperatures. Once the DMF is added, the reaction was maintained at 35 °C under constant stirring overnight, then the temperature of the reaction was increased and maintained first at 40°C for 4h and finally at 80 °C for 2h to complete the reaction. The reaction mixture was allowed to cool prior to the distillation process.

The residual $SOCl_2$ and DMF in the reaction mixture were removed by distillation at room temperature under vacuum. Then, 12 mL of toluene were added to the reaction mixture before the temperature was increased to 70 °C to complete the distillation

process. Finally, 12 mL of toluene were added, and the resulting viscous reaction solution was dissolved in 25 mL of hexane at 50 °C and maintained at 4 °C overnight to recrystallize. The recrystallized monomer was rinsed with 15 mL of hexane and maintained at 4 °C before vacuum drying under an inert atmosphere. The 6FCl monomer was purified by sublimation under vacuum at 60 °C for 2 h, 80 °C for 30 min, 100 °C for 1 h and 120 °C until sublimation was complete [26]. Likewise, the monomer APAF was purified by sublimation at 220 °C.

b) *Synthesis of the 6FCl-APAF polymer*

The synthesis of this polyimide was made by a modification of formation of polyamides by using the *in situ* silylation method [27,28] employing DMAP as activating promotor in a 3-neck flask, 3.56 g of the diamine APAF were added and dissolved in 19.5 mL of DMAc under an inert atmosphere (N_2). The mixture was mechanically stirred at room temperature until complete dissolution of the diamine. Then, the reaction temperature was lowered at 0 °C (by immersion of the 3-neck flask in an ice bath) before silylation by adding 4.94 mL of CTMS and 3.1314 mL of Py. Solvent was added slowly to avoid a sudden raise in the temperature of the reaction, which was maintained at 0 °C for 10 minutes after the addition of Py. The mixture was removed from the ice bath for 20 minutes and placed again prior addition of 4.1707 g of dichloride acid, and then 0.4749 g of DMAP. The polymer was allowed to react for 24 h at room temperature under gentle stirring. Then, 4 mL of DMAc were added to the polymerization reaction mixture, which was precipitated by slowly pouring into a beaker containing deionized water under vigorous magnetic agitation. The polymer fibers obtained were cleaned in deionized water for 1 h under gentle stirring. The polymer fibers were filtered in a Büchner funnel and maintained in an ethanol-water [40:60] solution at 50 °C for 2 h in order to extract

the solvents previously used. Finally, the fibers were filtered, dried at 100 °C overnight (without vacuum) and at 80 °C under vacuum for 24 h.

1.3 HPA membranes casting and their corresponding thermal rearranged materials (β-TR-PBO)

The polymeric membranes were prepared using a sequential dissolution-evaporation process by dissolving the above synthesized polymer in 10% of NMP (on a dry weight basis) in order to prepare the HPA, which was then filtered through a 3.1 µm fiberglass Symta (Symta, Madrid, Spain) filter before casting the solution. The HPA solution was poured into a glass ring located on well-leveled glass plate. The membranes were subjected to a heat treatment in order to remove progressively the solvent: 60 °C overnight followed by 2 h at 80 °C on the plate (without vacuum), 1 h at 100 °C, 2 h at 120 °C and finally 12 h at 180 °C under vacuum. The resulting membrane was slowly cooled down to room temperature.

An additional set of membranes was prepared as above described These precursor-HPA membranes were converted to β-TR-PBOs through a solid-state condensation reaction [26] by initially heating up to 250 °C at a rate of 5 °C/min, maintaining this temperature for 15 min, and further heating to 375 °C at a rate of 5 °C/min, maintaining this temperature for 15 min. The final temperature was defined according to the results of a dynamic thermogravimetric analysis of the HPA membrane.

Preparation of MMM and TR-MMM membranes

In order to prepare the mixed matrix membranes (MMMs), porous polymer networks (PPNs) were synthetized by combining Triptycene and 2,2,2-Trifluoroacetophenone (TFAP), according to the methodology described by Lopez-

Iglesias *et. al*. (2018) [29] (see Fig. 1). Triptycene and TFAP were added in a three-necked flask, stirred under a nitrogen atmosphere and cooled to 0°C. Then, trifluoromethanesulfonic acid (TFSA) was then added dropwise. The reaction was allowed to warm to room temperature and maintained at RT for 5 days under continuous stirring. The suspension reaction was poured onto an ethanol/water mixture and washed several times in this mixture, and finally it was dried under vacuum for 12 h at 150 ºC. The microporous materials obtained showed an outstanding thermal resistance (degradation temperature higher than 490 ºC), pore diameters greater than 0.45-0.50 nm and a specific surface area ranging higher than 550 m^2 /g.

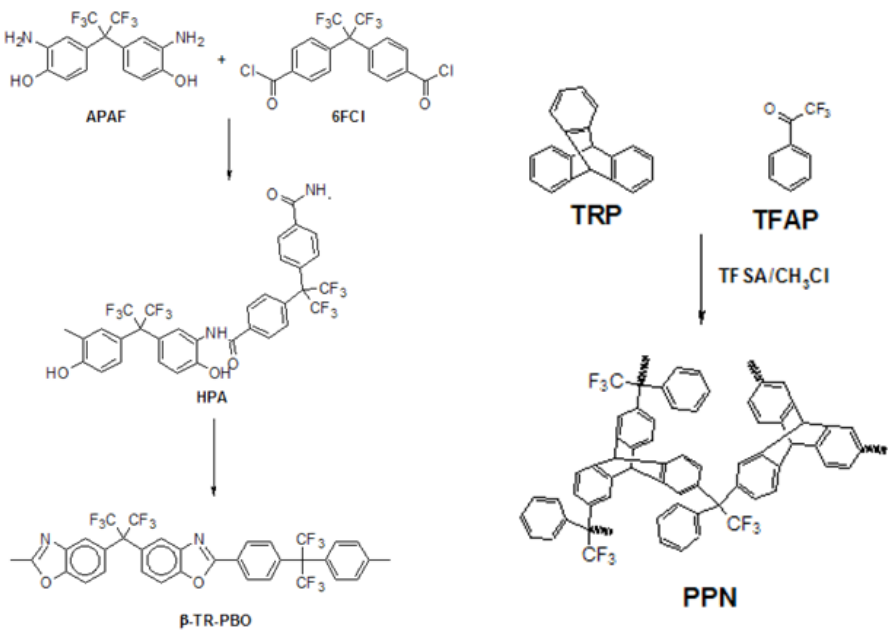

Fig. 1.- Scheme of the Synthesis of 6F-APAF (HPA and β-TR-PBO) (right) and synthesis of PPN (left).

An HPA solution was loaded with the PPN at 10, 15, 20, 30 and 40 % (on a dry weight basis). The procedure was as follows: 500 mg of HPA were diluted in 5 mL of NMP (10%) and filtered through a 3.1 µm fiberglass Symta filter (Symta, Madrid, Spain) before adding the PPN. For instance, a suspension with 10% of PPN (50 mg) was prepared in 0.5 mL of NMP. The suspension was stirred for 2 hours and then sonicated for 20 min

(40 cycles of 20 s sonication using 30% as maximum amplitude) with a 130 W ultrasonic probe Branson 450 Digital Sonifier (Marshall Scientific, Hampton, New Hampshire, USA) in order to disperse the particles completely. Then, the polymer solution was mixed with the sonicated PPNs, and this solution was maintained under stirring again for one hour before casting. The membranes were casted onto a well-leveled glass plate and were subjected to a heat treatment under vacuum in order to gradually remove the solvent: 60 °C overnight on the plate (without vacuum), 2 h at 80 °C/vacuum, 1 h at 100°C/vacuum, 2 h at 120 °C /vacuum and finally 12 h at 180°C/vacuum and slowly cooling down to room temperature. In order to establish the appropriate heat treatment conditions for the TR membranes, thermogravimetric analyses were performed. Thus, the membranes were treated at 375 ºC, following a thermal treatment under a nitrogen atmosphere with the ensuing steps: heating up to 250 °C at a rate of 5 °C/min, maintaining this temperature for 15 min, heating to 375 °C at a rate of 5 °C/min and maintaining this temperature for 15 min.

1.4 Characterization techniques

A complete characterization of the polymers requires the combination of information from multiple physical/chemical techniques in order to elucidate the structure of the materials under investigation, and to establish the limits of thermal stability, structure and the conditions for further material processing.

^{1}H and ^{13}C Nuclear Magnetic Resonance spectra (NMR) for monomers and polymers were carried out in a Varian AV (Agilent, Santa Clara, California, USA) working at 400 MHz and 100 MHz, respectively. Samples were prepared by dissolving approximately 10 mg in 0.6 mL of chloroform or deuterated dimethyl sulfoxide (DMSO-*d6*) as solvent.

The inherent viscosity of homopolyimides and copolyimides was measured at 30 °C using an automated Canon-Ubbelohde suspended level viscometer with NMP as the solvent. The polymer concentration was 0.5 g/dL. Weight-average molecular weight (M_w) and number-average molecular weight (M_n) of the polymeric matrix synthesized were determined by Gel Permeation Chromatography (GPC) using a Tosoh Ecosec HLC-8320GPC (Thoso, Shiba, Minato-Ku, Tokyo, Japan). Samples were prepared by dissolving 0.5 mg of each polymer in 2 mL of THF, the solution was filtered through a 0.45 µm filter prior introducing the solution in the injection vial.

Polymer solubility tests were carried out in order to determine the solvent to be used for membrane preparation. This was determined by placing ~ 10 mg of the polymer in 1 mL of the target solvent (DMAc, NMP, THF, $CHCl_3$, acetone, ethanol, DMF) in solubility tubes until its total dilution at room temperature. The heating above the solvent boiling point was applied to the membrane samples that were not readily dissolved at room temperature.

Thermal rearrangement process was carried out under a N_2 atmosphere in a Carbolite CTF 12/65/700 single-zone pyrolizer furnace.

The Attenuated Total Reflectance-Fourier Transform Infrared (ATR-FTIR) spectra, required to confirm conversion of HPA to TR-PBO, were monitored using a Spectrum One (Perkin Elmer, Waltham, Massachusetts, USA) FT-IR coupled with a universal Attenuated Total Reflection (ATR) sampling module with a diamond-tipped probe, following the band's intensity. All measurements were performed in the polymerics membranes, deposited on the crystal surface, by applying manual pressure on each sample. The interval of the 8 scans conducted ranged from 4000 to 250 cm^{-1}, with 4 cm^{-1} of resolution.

Thermogravimetric Analysis, isothermal and dynamic TGA were carried out using TA-Q-500 thermogravimetric analyzer (TA Instruments-Water Corp. Milford, Massachusetts, USA) under nitrogen flux (60 mL min^{-1}) at 10 °C min^{-1} in samples of about 5-10 mg in order to record the variations in HPA sample weight as a function of increasing temperature, which provided the thermal conditions for HPA conversion to β-TR-PBO.

Differential Scanning Calorimetry, DSC, was carried out in a TA Instruments DSC Q-20 Analyzer (TA Instruments-Water Corp. Milford, Massachusetts, USA) in order to monitor the glass transition temperatures (T_g). DSC analyses for TR polymers were carried out at a heating rate of 20 °C/min up to 360 °C, while for HPA polymers the use of modulated DSC (MDSC) was carried out at 20 °C/min up to 320 °C, under a N_2 atmosphere using 6-10 mg of membrane in gas-tight aluminum containers. The glass transition temperature, T_g, was determined in the second heating cycle, from the middle point of the resulting slopes.

The grade of order and the values of preferential MMMs and TR-MMMs membranes were investigated via wide-angle X-ray scattering, WAXS, at room temperature using a Bruker (Bruker, Billerica, Massachusetts, USA) D8 discover A25 advanced diffractometer equipped with a *Goebel* mirror. The LynxEye detector was operated at a speed of 0.5 seconds with a step scanning mode ranging from 5° to 70° and a 2θ step of 0.020°. A Cu Kα (λ = 1.542 Å) radiation source in a ceramic tube was used. Bragg's Law was used to determine the length spacing of the polymers (Eq. 1):

$$n\lambda = 2d\ sen\ \theta \quad (1)$$

where n is an integer. If a wavelength monochromatic X-ray beam strikes a crystal with an angle of incidence θ, the crystallographic planes of the samples, separated by a distance d, will reflect the X-rays.

The mechanical properties of MMMs and TR-MMM, which determine their applicability, were measured in a MTS Synergie-200 testing machine (MTS Systems, Eden Prairie, Minnesota, USA) equipped with a 10 N load cell. Rectangular pieces of 3.5 mm width and 25 mm length were cut from the membranes. Mechanical jaws were employed with an initial length of 10 mm between them and an extension speed of 5 mm/min. Six samples were tested for each polymer and MMM at room temperature.

Scanning electron microscopy, SEM, images were taken with a QUANTA 200 FEG ESEM (Thermo Fisher Scientific, Waltham, Massachusetts, USA) on Au-metallized samples operating at an acceleration voltage of 1.5 kV in high vacuum and using the detection of secondary electrons method. The samples were cryogenically fractured using liquid N_2 to obtain images of the cross section.

The fractional free volume, FFV, is defined as:

$$FFV = \frac{V - V_0}{V} \tag{2}$$

Here V is the total specific volume and V_0 is the specific skeletal volume of MMM. The skeletal volume for HPA, PPN and MMMs can be evaluated from their Van der Waals volumes because $V_0 \approx 1.3V_W$. The Van der Waals volumes can be correlated according to:

$$V_W^{MMM} = \phi V_W^{PPN} + (1-\phi)V_W^{HPA} \tag{3}$$

V_w^{HPA} and V_w^{PPN} were calculated by molecular modeling using the Materials Studio software (BioVia, San Diego, California, USA) and Eq. (3) allows to evaluate V_W^{MMM} and, correspondingly V_0^{MMM}. $\rho^{MMM} = 1/V^{MMM}$ and $\rho^{HPA} = 1/V^{HPA}$ were measured by following the Archimedes principle in a CP225 Analytical Balance from Sartorius (Sartorius, Göttingen, Germany) equipped with a density measurement kit. The samples were weighed in air and into high pure isooctane at room temperature. The average density from seven samples was obtained as:

$$\rho = \rho_0 \frac{W_{air}}{W_{air} - W_{C_8H_{18}}} \quad (4)$$

Where ρ_0 corresponds to the isooctane's density, W_{air} to the weight of the sample and $W_{C_8H_{18}}$ stands for the weight of the sample when submerged in isooctane. Finally, Eq. (2) allows the determination of FFV.

1.5 Gas Transport properties

The single gas permeability coefficients measurements for HPA, MMMs and TR-MMMs were determined using a constant volume/variable pressure apparatus at 35 °C and an upstream pressure of 3 bar, as described elsewhere [30]. In order to rule out the absence of pinholes in the membrane, helium permeability was measured at three different pressures (1, 2 and 3 bar) before starting the test of membrane in the permeation cell. Membranes were maintained overnight under vacuum before the determination of the permeability of N_2, O_2, CH_4 and CO_2, which were used to estimate the CO_2/CH_4 selectivity. The permeability coefficient (P), typically expressed in Barrer [1 barrer = 10^{-10} (cm^3 (STP) cm) / (cm^2 s cmHg) or, in SI units, 1 barrer = 3.35×10^{-16} (mol m)/(m^2 s Pa)], was obtained using the following expression:

$$P = \frac{273}{76}\frac{V\ell}{ATp_0}\left(\frac{dp}{dt}\right) \quad (5)$$

where V (cm^3) is the downstream volume, ℓ (cm) is the thickness of the membrane, A (cm^2) the effective area of the cell, T is the temperature in K, p_o is the upstream pressure (cm Hg) and dp(t)/dt accounts for the variation of the downstream pressure with time. The thickness of the membrane was measured before measurement of the permeability coefficient into the cell. The ideal selectivity for a gas pair was calculated from the ratio of their pure gas permeabilities P_A and P_B as follows:

$$\alpha_{A/B} = \frac{P_A}{P_B} \quad (6)$$

where P_A and P_B are the coefficients of the pure gases, A and B respectively.

2. Results and Discussion

2.1 Chemical properties

a) Characterization of the precursor poly (o-hidroxyamide), HPA.

The chemical structure of the HPA was also evaluated prior to this work [15], where the signals of the amino and hydroxyl groups (at ~10 ppm (δNH*)* and ~9.50 ppm (δOH), respectively) were confirmed by NMR. In addition, the activation of the aromatic ring by the hydroxyl group, identified by resonance in the high fields (δ ~7.0 ppm) of the aromatic protons *ortho* to the phenolic OH, was observed.

The inherent viscosity obtained for HPA was 0.82 dL/g. This could be taken as an indicative of the relatively high molecular weight of this polymer. By GPC a weight-average molecular weight M_w =161354 Dalton was obtained.

Solubilities are shown in Table I. The polymer solubility was studied using different solvents. The polymer was soluble in common organic solvents such as THF and acetone, and polar aprotic solvents such as DMAc, NMP, DFM, but not in $CHCl_3$, DMSO and ethanol. In this work, NMP has been used as solvent.

Table I.- Solubility of 6FCl-APAF.

DMAc	**NMP**	**THF**	**$CHCl_3$**	**Acetone**	**Ethanol**	**DMF**	**DMSO**
++	++	++	-	+	-	++	-

++ soluble, + soluble upon heating, +- partially soluble, - insoluble

b) Infrared Spectroscopy (FTIR) measurements

Infrared spectra measurements were used to confirm the chemical structure of the processed polymers. This technique allowed assigning the characteristic bands of the functional groups, also confirming the conversion to benzoxazole in the thermally rearranged TR-MMMs obtained. FT-IR spectra showed the absorption bands recorded for the family of the MMMs and the corresponding thermal rearrangements, using HPA as a reference of the effect produced by the PPN loading (Fig. 2). These spectra were measured for MMM membranes heated at 180°C. The C=O bond was identified by the stretching vibration bands recorded at 1657 cm^{-1} and N-H symmetric band at 1498 cm^{-1}. The transformation of MMM into β-TR-PBO was observed by the decrease in the characteristic band of the carboxamide group (at 1657 cm^{-1}), and the absence of effects in the transverse stretching band of C-N-C at 1200 cm^{-1}. Finally, the presence of the bands

at 1480 and 1058 cm^{-1} confirmed that the thermal conversion to polybenzoxazole was successful.

The carbonyl group about 1700 cm^{-1} was not observed in the MMMs doped with different percentages of PPNs. In addition, the absorption stretch band of the C-F group was observed at ~ 1200 cm^{-1} absorption peak. In addition, the absorption band at 1433 cm^{-1}, confirmed the presence of the filler (PPN) in the MMMs. The broad band in the MMM spectra, in the region between 3500-3000 cm^{-1}, was attributed to the O-H vibration of the hydroxy groups [31], while thermal restructuring with the absence of the OH group was observed in their corresponding β-TR-PBO.

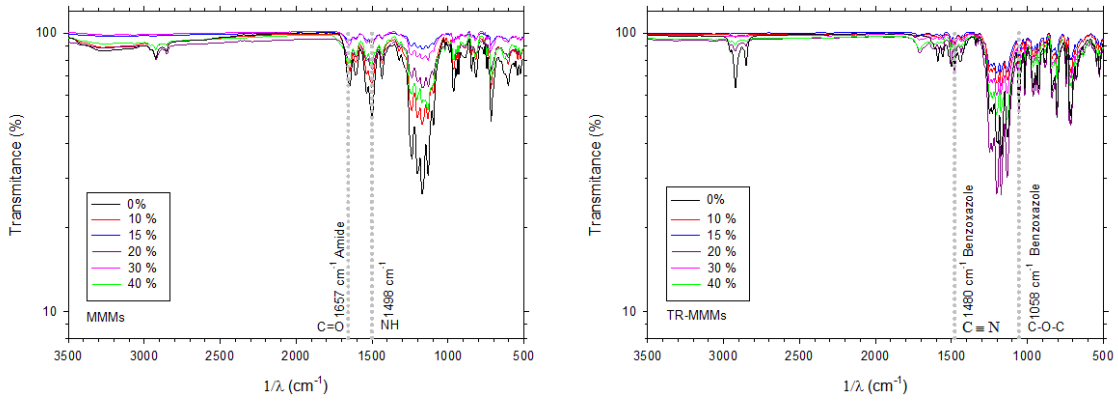

Fig. 2. ATR-FTIR spectra of precursor MMM with 0, 10, 15, 20, 30 and 40 % of PPN (left) and the corresponding TR-MMMs.

c) WAXS

X-Ray scattering (WAXS) spectra are shown in Fig. 3, showing that the polymers are essentially amorphous.

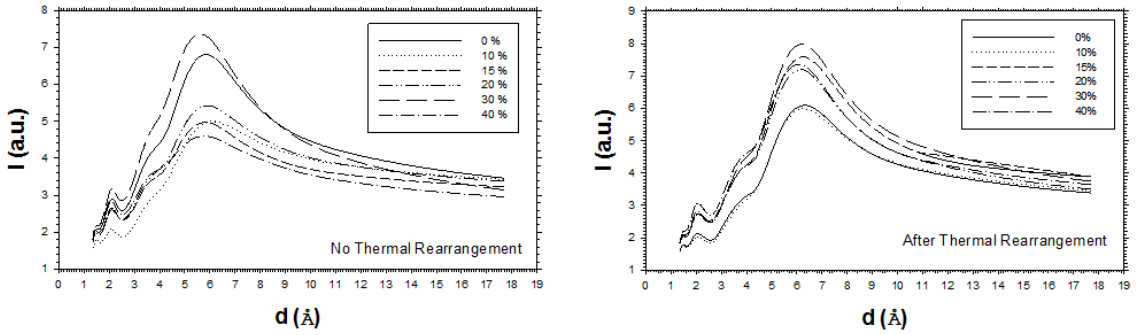

Fig. 3.- WAXS spectra for the studied membranes before (left) and after (right) thermal rearrangement.

The evolution of the most probable intersegmental distances, δ_{max}, are shown in Fig. 4 as a function of the PPN content. It seems clear that δ_{max} decreases slightly when the amount of PPN increases in the membrane. Given that pure PPN has a higher intersegmental distance [29], the trend could only be explained by a small compaction of the polymeric matrix due to the presence of PPN. Thermal rearrangement increases δ_{max}, which should lead to increasing FFV.

It is worth noting that the total range of d-spaces appearing in Fig 4 span from 5.6 to 6.4 while all δ_{max} distributions are than 5 Angstrom wide. Thus, the tendency shown in Fig. 4 refers to maxima in δ_{max} appearing among many other chain-to-chain lengths as corresponding to amorphous materials.

Note that δ_{max} of HPA is more dispersed than after thermal rearrangement, probably due to the presence of residual solvent, which is especially difficult to eliminate from HPAs. In addition, PPN has solvent inside the pores, and solvent removal from both the matrix and the filler is not easy, without achieving a measurable conversion to PBO. However, TR conversion eliminates all residual solvent giving a smoother dependence of δ_{max} on the PPN content. This feature will appear for many magnitudes analyzed here.

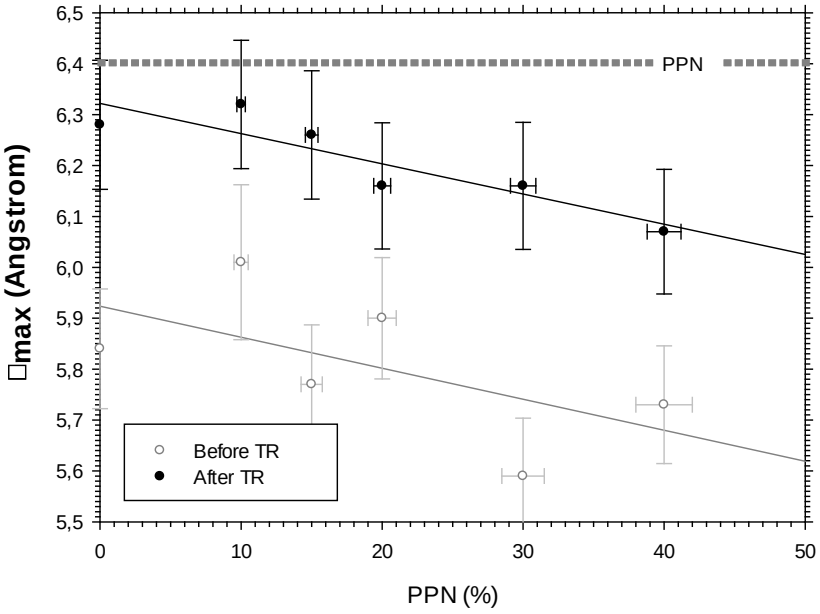

Fig. 4.- Intersegmental distances according to WAXS before and after thermal rearranging.

2.2 Morphology of the MMMs

a) Scanning Electron Microscopy

The SEM images taken from the cross section of the MMMs and TR-MMMs membranes containing PPN at 10, 20 and 40 wt. % showed a decreasing, but fair enough, compatibility between the HPA 6FCl-APAF and the PPNs particles as shown in Fig. 5. Moreover, a change in the morphology of the membranes was observed after thermal rearrangement, which could probably be due to the total loss of both water and residual solvent in the structural unit of the membrane caused by the high temperature used during thermal rearrangement.

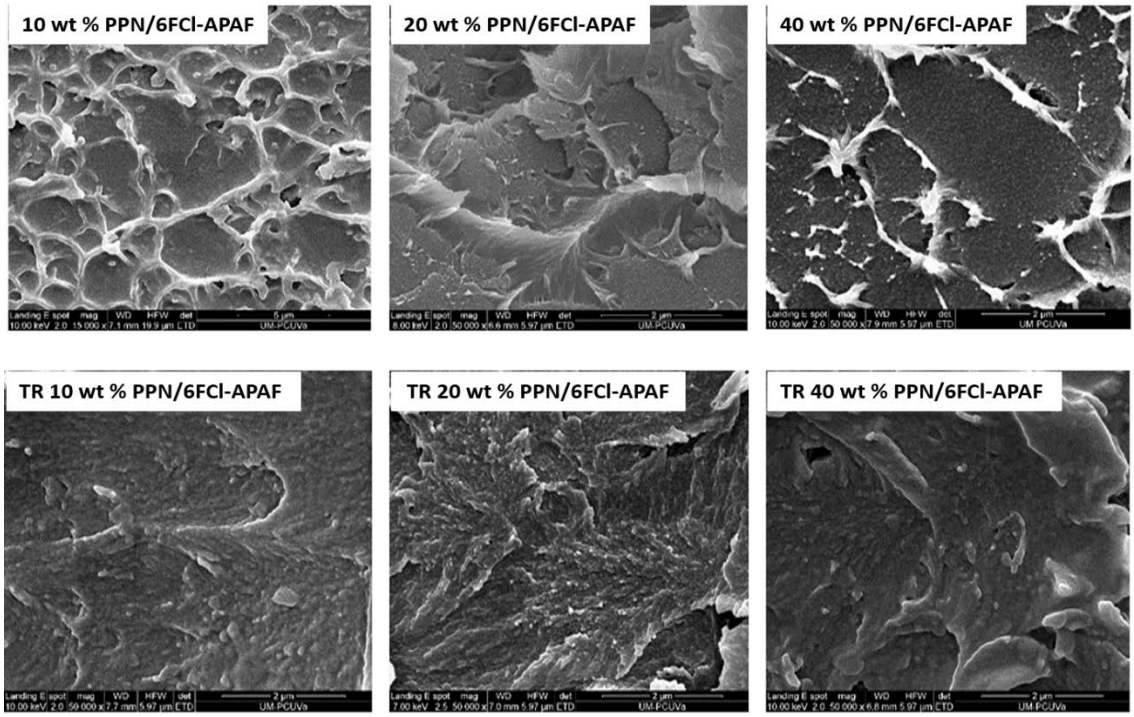

Fig. 5.- SEM pictures of the morphology of MMMs (up) and TR-MMMs (down) containing 10 %, 20 % and 40 % (from left to right).

b) Fractional free volume (FFV)

Fig. 6 shows, on the left, the decrease in FFV for both MMMs and TR-MMMs when the PPN load increases. On the right, $\Delta FFV=(FFV_{TR}-FFV)/FFV$ is shown versus PPN content. There, it can be seen that the relative effect of thermal rearrangement on FFV seems to be facilitated by the presence of the PPN filler.

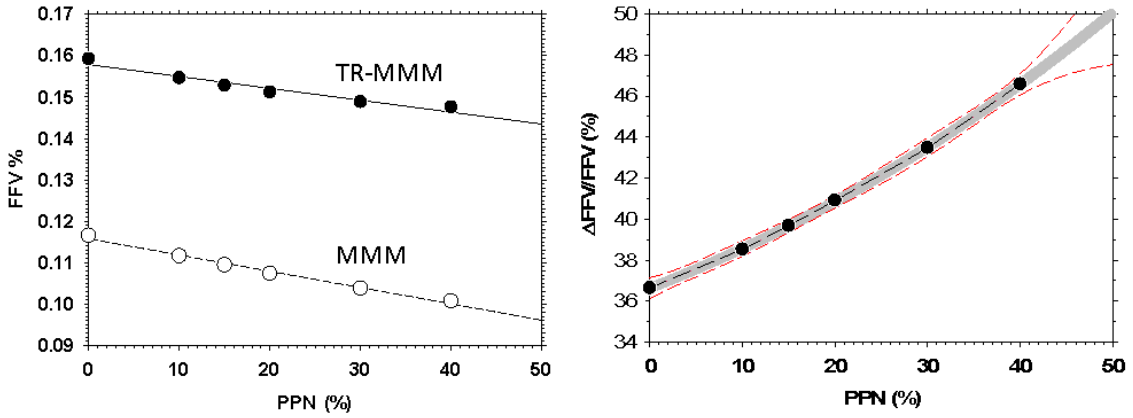

Fig. 6.- FFV (left) for MMMs and TR-MMMs, and ΔFFV=(FFV$_{TR}$-FFV)/FFV (right)as a function of PPN mass fraction.

The decrease of FFV for higher PPN fractions should be due to the lower free volume contributed by PPN. The effectiveness of thermal rearrangement to increase FFV seems to be favored by the presence of PPN. This could indicate that some extra FFV would appear by the interfaces between PPN and the polymeric matrix more efficiently due to the thermal treatment.

2.3 Thermal properties

a) Thermogravimetric analysis (TGA).

TGA scans of the membranes were performed in order to characterize their thermal stabilities. Fig. 7 depicts the thermograms with the different weight losses for HPA and MMM before thermal rearrangement. These analyses show a typical two-stage weight loss [32]. The first weight loss is due to the thermal rearrangement process, and the second one could be associated with the generalized thermal degradation of the material [33]. In our study, the membranes without thermal rearrangement experienced a weight loss under 100 ºC related with moisture removal (~5-10 %). The second weight loss between 200 and 400 ºC was likely related with the evaporation of residual solvent (~14 %) which is complex to remove due to the nature of the HPA. Because the weight loss from 375 to 400 ºC was quite low and fast, as confirmed by isothermal TGA

measurements, thermal rearrangement should happen around 375 ºC after short residence times (around 15 min) without any residual solvent left. Finally, polymer degradation starts at temperatures above 450 ºC. It is worth noting that PPN degradation occurs at 490 ºC in N_2 [29].

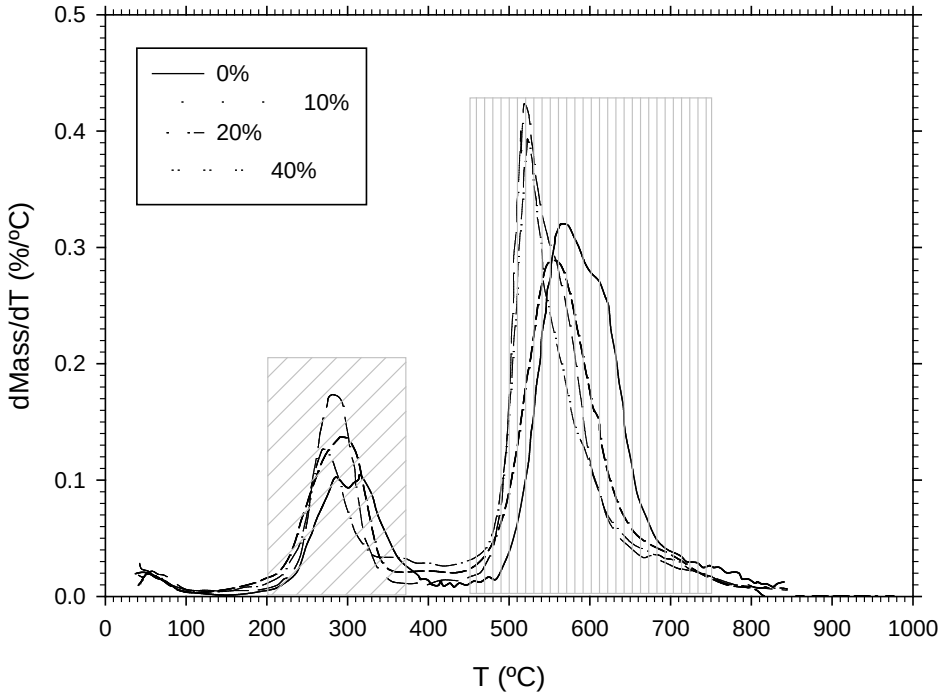

Fig. 7.- Differential thermogravimetric analysis of HPA-MMMs. Samples were heated from 50 to 800 °C at 5 °C/min in a N_2 atmosphere.

The TGAs analysis in TR-MMM samples confirmed the high stability conferred by both thermal rearrangement and PPN loading leading to an almost equal weight loss linked to degradation of the thermally formed TR-MMMs.

b) DSC for glass transition temperatures

The obtained T_g are shown in Fig. 8 versus the PPN percentage of both MMMs and TR-MMMs. T_g, (and consequently rigidity) is observed to increase both after thermal rearrangement and with increasing PPN content.

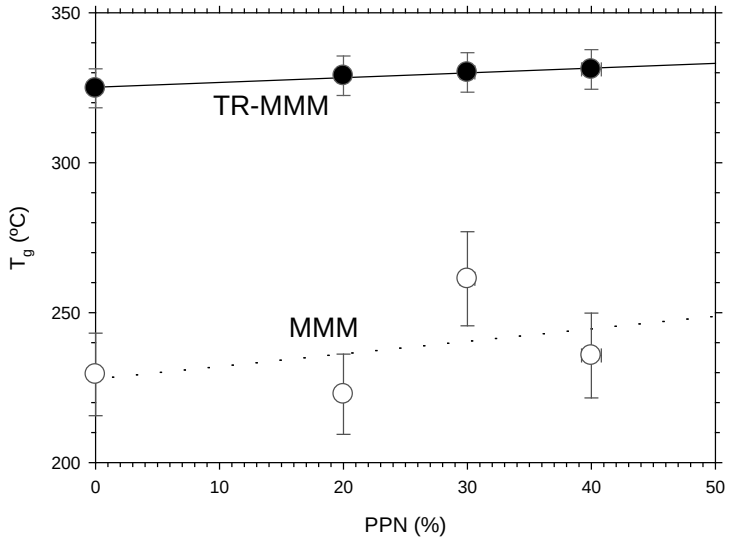

Fig. 8.- T_g versus PPN content of the MMM and TR-MMM membranes.

It is worth noting that the increase in rigidity when PPN content increases happens simultaneously with a decrease in fractional free volume as shown in Fig. 6 (left). Note that, it has mentioned when commenting on δ_{max} (in section 2.1.c), the remarkable dispersion of T_g before thermal rearrangement could be due to the presence of residual solvent that would be totally eliminated only after thermal rearrangement.

2.4 Mechanical properties

Mechanical properties are good enough and relatively worse both after thermal rearrangement and when PPN content increases as seen in Fig. 9. This agrees with the increase of rigidity detected by DSC.

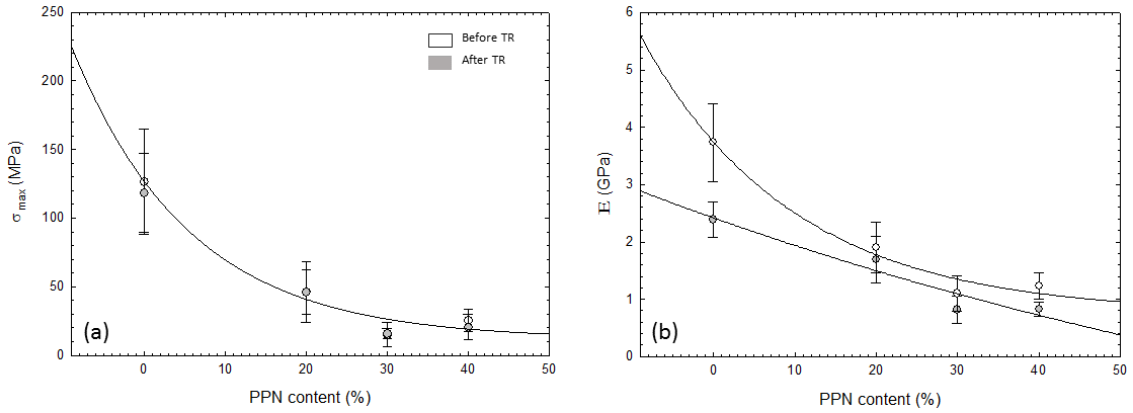

Fig. 9.- Maximal bearable stress (a) and Young modulus (b) for our membranes before and after thermal treatment as a function of PPN content.

2.5 Gas separation properties

Ideal gas transport permeabilities (P) of He, N_2, O_2, CH_4 and CO_2 at 3 bar (300kPa) and 35°C for the precursor membranes of the MMMs and their β-TR-PBO counterparts were measured, along with the ideal selectivity (α) for some gas pairs, as shown in Table II.

Table II. Permeability Coefficients (Barrer) at 3 bar (300 kPa) and 35 ºC for MMMs and their corresponding TR-MMMs.*

Membrane	**Permeabilities (Barrer*)**					**Ideal selectivities**	
	He	**N_2**	**O_2**	**CH_4**	**CO_2**	**$\alpha O_2/N_2$**	**$\alpha CO_2/CH_4$**
HPA (0 %)	43.61	0.46	2.48	0.19	9.28	5.36	50.01
MMM -10 %	47.84	0.48	2.58	0.21	9.20	5.34	44.09
MMM -15 %	56.28	0.65	3.64	0.29	13.73	5.63	47.91
MMM -20 %	60.07	0.89	4.62	0.46	18.28	5.17	40.01
MMM -30 %	222.07	4.54	22.87	2.05	93.03	5.04	45.41
MMM -40 %	37.01	0.49	2.58	0.42	13.95	5.33	32.95
TR-HPA (0 %)	244.61	10.88	44.74	6.72	186.59	4.11	27.75
TR-MMM-10 %	245.96	11.13	45.88	7.36	202.68	4.12	27.53
TR-MMM-15 %	364.18	16.27	67.67	10.64	288.20	4.16	27.09
TR-MMM-20 %	355.16	20.35	82.29	14.26	351.32	4.04	24.63
TR-MMM-30 %	708.57	43.40	172.06	32.85	789.06	3.96	24.02
TR-MMM-40 %	288.34	19.93	71.18	15.47	300.52	3.57	19.42

* 1 Barrer=10^{-10} cm^3(STP) cm /cm^2. s. cmHg or, in SI units, 1 barrer = 3.35×10^{-16} (mol m) / (m^2 s Pa).

The Robeson's plot [34] (double log plot of selectivity versus permeability of the most permeable gas for a given gas pair) for the CO_2/CH_4 is shown in Fig. 10. It seems clear that because of thermal rearrangement, permeability increases notably with just a slight decrease of selectivity. It can be seen also that, both before and after thermal rearrangement, the highest permeability value was observed for the TR-MMM filled with 30 % PPN. Remarkably, the TR-MMM loaded with 40 % of PPN showed a decrease both in permeability and selectivity for all gases when compared to those expected attending to the tendencies up to 30 % PPN. If pure polymeric matrix membranes are compared with those containing 40 % PPN a decrease in selectivity with an increase in permeability are seen. This phenomenon is well known and was described already by Moore and Koros in 2005 [35] and more recently by Galizia et al [36] and could be explained as an intensification of the same phenomena explaining the increase of permeability and the (in these cases small) decrease in selectivity observed for PPN contents until 30 %.

It is worth mentioning that there are significant variations in permeability and selectivity for the membranes without thermal rearrangement that could be attributed to the presence of variable small amounts of solvent retained within both the polymeric matrix [15] and the PPN filler.

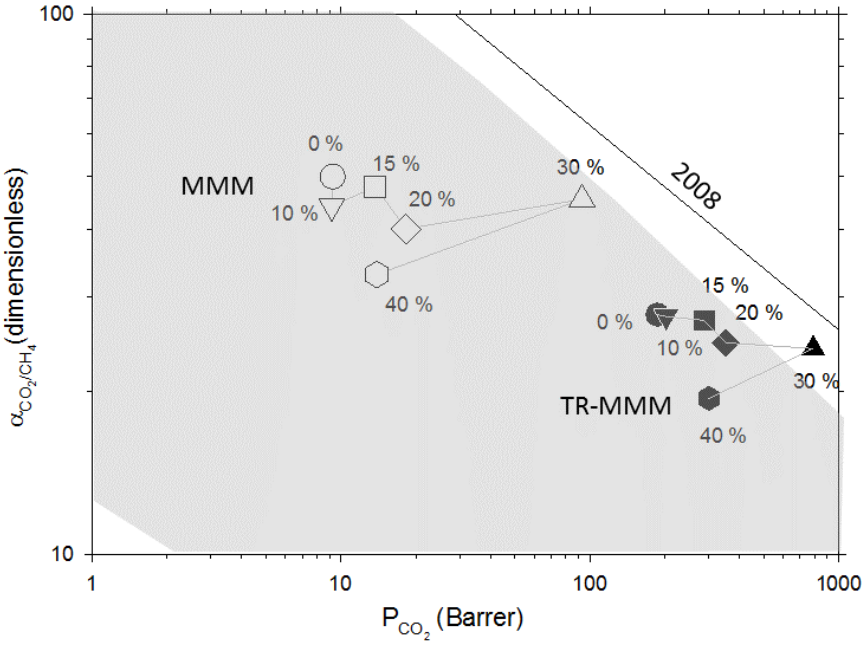

Fig. 10.- Robeson plot for the MMMs and TR-MMMs studied here. The shaded area corresponds to the highest presence of polymers studied by Robeson. The straight line corresponds to the upper bond given by Robeson in 2008 [34].

In Fig. 11, the CO_2 diffusivity and solubility are shown. The figure shows that, both before and after thermal rearrangement, diffusivity increases, and solubility decreases, when the PPN load increases. After thermal rearrangement both diffusivity and solubility (and consequently permeability) area higher. In this Fig. 11, it is also seen that solubility decreases both before and after thermal rearrangement steeply when PPN load reaches 40 %.

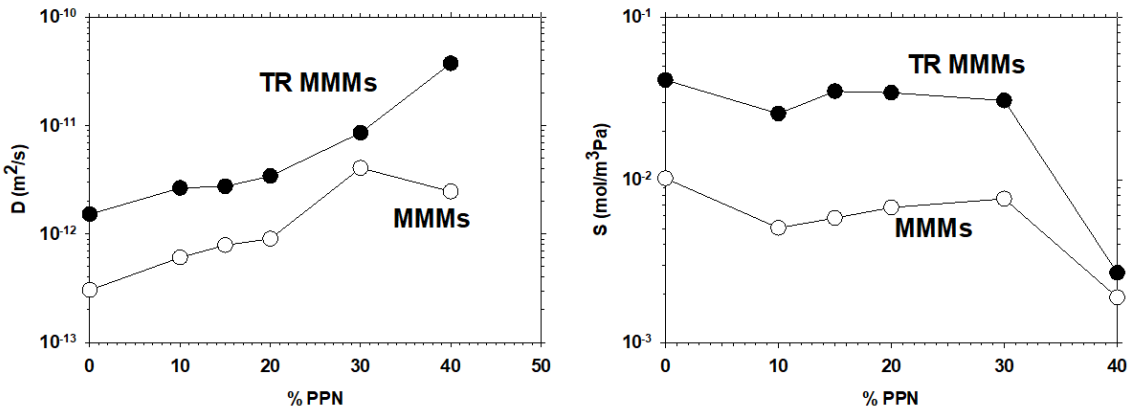

Fig. 11.- CO_2 diffusivity and solubility for PPN contents from 0 to 40 %.

Concerning selectivity, a separate analysis of the influence of both diffusive and solubility selectivities can be done by defining diffusion selectivity and solubility selectivity as:

$$\alpha_{A/B} = \frac{D_A}{D_B}\left(\frac{S_A}{S_B}\right) = \alpha^D_{A/B}\alpha^S_{A/B} \tag{7}$$

This has been done in accordance with Eq. (6) and considering that $P_i = D_i S_i$.

In Fig. 12, both the selectivities $\alpha^D_{CO_2/CH_4}$ and $\alpha^S_{CO_2/CH_4}$ along with the overall one α_{CO_2/CH_4}, are shown. It appears clear that, for both MMMs and TR-MMMs, the CO_2/CH_4 selectivity slightly decreases when the fraction of PPN increases. Nevertheless, in MMMs the diffusion selectivity increases, and the solubility selectivity decreases, while in TR-MMMs the opposite tendency is seen.

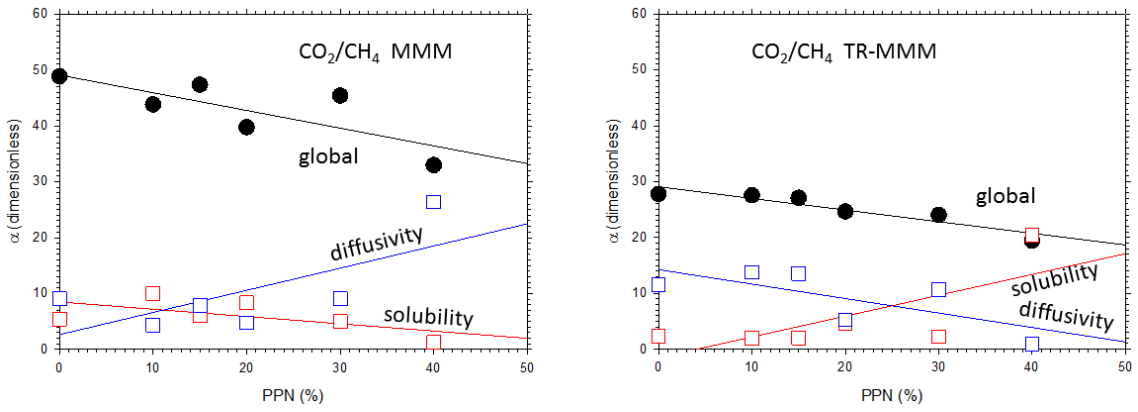

Fig. 12.- Overall, diffusive and solubility selectivities for the CO_2/CH_4 pair of gases. MMMs results are shown on the left and TR-MMMs data are shown on the right.

This behavior means that the global selectivity fall in MMMs could be due to

solubility effects, while diffusion changes would dominate the overall selectivity for TR-MMMs. This could be interpreted in terms of an increase of FFV caused by the thermal rearrangement that would change the size distribution of FFV voids. Before thermal rearrangement the addition of PPN would decrease FFV, decreasing void-to-void necks, discriminating between CO_2 and CH4 size. At the same time, their internal volumes would increase, to make their inner surfaces more accessible to both CO_2 and CH_4. After thermal rearrangement, the addition of PPN would widen necks, allowing both CO_2 and CH_4 pass more similarly, and decrease internal volumes to allow CO_2 to adsorb better than CH_4.

It has already been noted that thermal rearrangement should increase rigidity and intersegmental distances (see Fig. 4 and Fig. 7), these interpretations seem reasonable. Also, the addition of PPN decreases intersegmental distances and increases rigidity with permeability rise due to increases in the internal volumes of the voids, before thermal rearrangement, or to increases in the size of void-to-void channels, both compatible with an overall decrease of FFV.

Permeability could also increase due to extra free volume due to PPN-HPA interfaces that could increase the permeability without any relevant contribution to selectivity. Actually, the Robeson's plot (see Fig. 10), according to the classification made by Moore and Koros [35] seems compatible with their Cases II and III where there appear voids at the interfaces. The highest permeability appeared at 30 % PPN. This could be attributed to a balance between the enlargement of PPN-HPA interfaces and the presence of PPN conglomerates decreasing these interfaces.

3. Conclusions

Mixed matrix membranes, MMMs, consisting in variable loads of a porous polymer network, PPN, into a o-hydroxypolyamide, HPA, were thermally treated to induce the transformation of HPA to a polybenzoxazole (β-TR-PBO). The HPA chosen in this work was 6FCl-APAF while the load consisted in different percentages of a PPN synthetized by combining triptycene and trifluoroacetophenone. The resulting MMMs showed high thermally stability, degradation temperature higher than 450 ºC, and they could be processed to TR-MMM (β-TR-PBO-PPN) materials by thermal rearrangement at 375 ºC for 15 min.

The most probable intersegmental distances, δ_{max} decreases slightly when the amount of PPN increases. This could be explained by a small compaction of the polymeric matrix induced by the presence of PPN because it has intersegmental distances over those of the polymeric matrix. This compaction should be reduced by the TR process with the subsequent increase in δ_{max} .

Free volume fractions, FFV, decrease for higher PPN content. The increase of FFV due to thermal rearrangement seems to be favored by the presence of the PPN load. This could indicate that some extra FFV appear in the interfaces between PPN and the polymeric matrix after the thermal treatment. Rigidity increases (T_g increases) when PPN content increases both before and after thermal rearrangement and is much higher after thermal rearrangement. Mechanical properties were good enough as to allowing film handling and membrane operation.

CO_2/CH_4 selectivity decreases slightly when the PPN content increases and also as a consequence of thermal rearrangement. CO_2 permeability increases after thermal

rearrangement and, both before and after thermal rearrangement, it grows when the content of PPN rises until 30 % with a sharp fall at 40 % PPN. It seems that selectivity decreases in MMMs due to solubility effects, while diffusivity changes make selectivity to decline for TR-MMMs. Because solubility is mainly linked to internal surfaces while diffusivity has to do with inter-cavity paths, we can suggest that thermal rearrangement would change the body-to-neck balance of voids. The inclusion of PPN would decrease FFV widening void-to-void communication and increasing their internal surfaces before thermal rearrangement. Thermal rearrangement would widen necks and reduce internal surfaces.

The addition of PPN increases internal surfaces of the voids and/or the size of void-to-void channel with an overall decrease of FFV and compaction of the polymeric matrix. It could also appear extra FFV (not detected by the procedures used here to get it) with the subsequent contribution to permeability without changes in selectivity. The maximal permeability for PPN contents around 30 % could be attributed to a balance between the enlargement of PPN-HPA interfaces and the appearance of PPN conglomerates blocking these interfaces.

In summary, these new MMM membranes show good thermal stability, enough mechanical properties, showing very high CO_2 permeabilities with good values of CO_2/CH_4 selectivities.

4. Acknowledgements

This work was supported by the Spanish Government (AEI) through projects MAT2016-76413-C2-1-R and MAT2016-76413-C2-2-R and by the Regional Government of Castilla y León and the EU-FEDER program (CLU2017-09, UIC082, VA088G19 and PhD grant of Cenit Soto). We are grateful to Salvador Azpeleta (LTI,

University of Valladolid) for performing the WAXS measurements.

5. References

[1] S. Achinas, V. Achinas, G.J.W. Euverink, A Technological Overview of Biogas Production from Biowaste, Engineering. 3 (2017) 299–307. https://doi.org/10.1016/J.ENG.2017.03.002.

[2] IEA, WEO-2017 Special Report: Energy Access Outlook, (2017) 1–143. https://doi.org/ceo871024 [pii].

[3] European Biogas Association, EBA' s biomethane fact sheet, (2013) 1–4.

[4] European Biogas Association, EBA Statistical Report 2018, Annu. Rep. (2018) 68. https://doi.org/10.1139/e11-014.

[5] I. Angelidaki, L. Treu, P. Tsapekos, G. Luo, S. Campanaro, H. Wenzel, P.G. Kougias, Biogas upgrading and utilization: Current status and perspectives, Biotechnol. Adv. 36 (2018) 452–466. https://doi.org/10.1016/j.biotechadv.2018.01.011.

[6] A. Toledo-Cervantes, J.M. Estrada, R. Lebrero, R. Muñoz, A comparative analysis of biogas upgrading technologies: Photosynthetic vs physical/chemical processes, Algal Res. 25 (2017) 237–243. https://doi.org/10.1016/J.ALGAL.2017.05.006.

[7] A. Petersson, A. Wellinger, Biogas upgrading technologies – developments and innovations Task 37 -Energy from biogas and landfill gas IeA Bioenergy aims to accelerate the use of environmental sound and cost-competitive Bioenergy on a sustainable basis, and thereby achieve a substant, IEA Bioenergy. (2009) 13. http://www.build-a-biogas-plant.com/PDF/IEA_Biogas_technologies.pdf.

[8] F. Bauer, C. Hulteberg, T. Persson, D. Tamm, Biogas upgrading – Review of commercial technologies., (2013). http://www.sgc.se/ckfinder/userfiles/files/SGC270.pdf.

[9] R. Muñoz, L. Meier, I. Diaz, D. Jeison, A review on the state-of-the-art of physical/chemical and biological technologies for biogas upgrading, Rev. Environ. Sci. Biotechnol. 14 (2015) 727–759. https://doi.org/10.1007/s11157-015-9379-1.

[10] I. Ullah Khan, M. Hafiz Dzarfan Othman, H. Hashim, T. Matsuura, A.F. Ismail, M. Rezaei-DashtArzhandi, I. Wan Azelee, Biogas as a renewable energy fuel – A review of biogas upgrading, utilisation and storage, Energy Convers. Manag. 150 (2017) 277–294. https://doi.org/10.1016/J.ENCONMAN.2017.08.035.

[11] I. Angelidaki, L. Treu, P. Tsapekos, G. Luo, S. Campanaro, H. Wenzel, P.G. Kougias, Biogas upgrading and utilization: Current status and perspectives, Biotechnol. Adv. 36 (2018) 452–466. https://doi.org/10.1016/J.BIOTECHADV.2018.01.011.

[12] S. Li, H.J. Jo, S.H. Han, C.H. Park, S. Kim, P.M. Budd, Y.M. Lee, Mechanically robust thermally rearranged (TR) polymer membranes with spirobisindane for gas separation, J. Memb. Sci. 434 (2013) 137–147. https://doi.org/10.1016/j.memsci.2013.01.011.

[13] M. Etxeberria-Benavides, O. David, T. Johnson, M.M. Łozińska, A. Orsi, P.A. Wright, S. Mastel, R. Hillenbrand, F. Kapteijn, J. Gascon, High performance mixed matrix membranes (MMMs) composed of ZIF-94 filler and 6FDA-DAM polymer, J. Memb. Sci. 550 (2018) 198–207. https://doi.org/10.1016/J.MEMSCI.2017.12.033.

[14] A. Tena, M. de la Viuda, L. Palacio, P. Prádanos, Á. Marcos-Fernández, Á.E. Lozano, A. Hernández, Prediction of gas permeability of block-segregated polymeric membranes by an effective medium model, J. Memb. Sci. 453 (2014) 27–35. https://doi.org/10.1016/j.memsci.2013.10.023.

[15] B. Díez, P. Cuadrado, Á. Marcos-Fernández, J.G. de la Campa, A. Tena, P. Prádanos, L. Palacio, Y.M. Lee, C. Alvarez, Á.E. Lozano, A. Hernández, Thermally rearranged polybenzoxazoles made from poly(ortho-hydroxyamide)s. Characterization and evaluation as gas separation membranes, React. Funct. Polym. 127 (2018) 38–47. https://doi.org/10.1016/j.reactfunctpolym.2018.03.013.

[16] O.G. Nik, X.Y. Chen, S. Kaliaguine, Functionalized metal organic framework-polyimide mixed matrix membranes for CO 2/CH 4 separation, J. Memb. Sci. 413–414 (2012) 48–61. https://doi.org/10.1016/j.memsci.2012.04.003.

[17] H.B. Park, S.H. Han, C.H. Jung, Y.M. Lee, A.J. Hill, Thermally rearranged (TR) polymer membranes for CO2 separation, J. Memb. Sci. 359 (2010) 11–24. https://doi.org/10.1016/J.MEMSCI.2009.09.037.

[18] T. Ben, H. Ren, M. Shengqian, D. Cao, J. Lan, X. Jing, W. Wang, J. Xu, F. Deng, J.M. Simmons, S. Qiu, G. Zhu, Targeted synthesis of a porous aromatic framework with high stability and exceptionally high surface area, Angew. Chemie - Int. Ed. 48 (2009) 9457–9460. https://doi.org/10.1002/anie.200904637.

[19] K. Konstas, J.W. Taylor, A.W. Thornton, C.M. Doherty, W.X. Lim, T.J. Bastow, D.F. Kennedy, C.D. Wood, B.J. Cox, J.M. Hill, A.J. Hill, M.R. Hill, Lithiated porous aromatic frameworks with exceptional gas storage capacity, Angew. Chemie - Int. Ed. 51 (2012) 6639–6642. https://doi.org/10.1002/anie.201201381.

[20] A.O. Malakhov, S.D. Bazhenov, V.P. Vasilevsky, I.L. Borisov, A.A. Ovcharova, A.V. Bildyukevich, V.V. Volkov, L. Giorno, A.V. Volkov, Thin-film composite hollow fiber membranes for ethylene/ethane separation in gas-liquid membrane contactor, Sep. Purif. Technol. 219 (2019) 64–73. https://doi.org/10.1016/j.seppur.2019.02.053.

[21] X.Q. Cheng, K. Konstas, C.M. Doherty, C.D. Wood, X. Mulet, Z. Xie, D. Ng, M.R. Hill, L. Shao, C.H. Lau, Hyper-Cross-Linked Additives that Impede Aging and Enhance Permeability in Thin Polyacetylene Films for Organic Solvent Nanofiltration, ACS Appl. Mater. Interfaces. 9 (2017) 14401–14408. https://doi.org/10.1021/acsami.7b02295.

[22] C.H. Lau, X. Mulet, K. Konstas, C.M. Doherty, M.A. Sani, F. Separovic, M.R. Hill, C.D. Wood, Hypercrosslinked additives for ageless gas-separation membranes, Angew. Chemie - Int. Ed. 55 (2016) 1998–2001. https://doi.org/10.1002/anie.201508070.

[23] M.R. Khdhayyer, E. Esposito, A. Fuoco, M. Monteleone, L. Giorno, J.C. Jansen, M.P. Attfield, P.M. Budd, Mixed matrix membranes based on UiO-66 MOFs in the polymer of intrinsic microporosity PIM-1, Sep. Purif. Technol. 173 (2017) 304–313. https://doi.org/10.1016/J.SEPPUR.2016.09.036.

[24] J.S. Kim, S.J. Moon, H.H. Wang, S. Kim, Y.M. Lee, Mixed matrix membranes with a thermally rearranged polymer and ZIF-8 for hydrogen separation, J. Memb. Sci. 582 (2019) 381–390. https://doi.org/10.1016/J.MEMSCI.2019.04.029.

[25] S.J.D. Smith, R. Hou, C.H. Lau, K. Konstas, M. Kitchin, G. Dong, J. Lee, W.H. Lee, J.G. Seong, Y.M. Lee, M.R. Hill, Highly permeable Thermally Rearranged Mixed Matrix Membranes (TR-MMM), J. Memb. Sci. (2019). https://doi.org/10.1016/j.memsci.2019.05.046.

[26] Z.P. Smith, K. Czenkusch, S. Wi, K.L. Gleason, G. Hernández, C.M. Doherty, K. Konstas, T.J. Bastow, C. Álvarez, A.J. Hill, A.E. Lozano, D.R. Paul, B.D. Freeman, Investigation of the chemical and morphological structure of thermally rearranged polymers, Polymer (Guildf). 55 (2014) 6649–6657. https://doi.org/10.1016/j.polymer.2014.10.055.

[27] D.M. Muñoz, J.G. De La Campa, J. De Abajo, A.E. Lozano, Experimental and theoretical study of an improved activated polycondensation method for aromatic polyimides, Macromolecules. 40 (2007) 8225–8232. https://doi.org/10.1021/ma070842j.

[28] A.E. Lozano, J. de Abajo, J.G. de la Campa, Synthesis of aromatic polyisophthalamides by in situ silylation of aromatic diamines, Macromolecules. 30 (1997) 2507–2508. https://doi.org/10.1021/ma961543p.

[29] B. Lopez-Iglesias, F. Suárez-García, C. Aguilar-Lugo, A. González Ortega, C. Bartolomé, J.M. Martínez-Ilarduya, J.G. De La Campa, Á.E. Lozano, C. Álvarez, Microporous Polymer Networks for Carbon Capture Applications, ACS Appl. Mater. Interfaces. 10 (2018) 26195–26205. https://doi.org/10.1021/acsami.8b05854.

[30] R. Recio, L. Palacio, P. Prádanos, A. Hernández, Á.E. Lozano, Á. Marcos, J.G. de la Campa, J. de Abajo, Gas separation of 6FDA-6FpDA membranes. Effect of the solvent on polymer surfaces and permselectivity, J. Memb. Sci. 293 (2007) 22–28. https://doi.org/10.1016/j.memsci.2007.01.022.

[31] B. Comesaña-Gándara, M. Calle, H.J. Jo, A. Hernández, J.G. de la Campa, J. de Abajo, A.E. Lozano, Y.M. Lee, Thermally rearranged polybenzoxazoles membranes with biphenyl moieties: Monomer isomeric effect, J. Memb. Sci. 450 (2014) 369–379. https://doi.org/10.1016/J.MEMSCI.2013.09.010.

[32] S.H. Han, J. Kwon, Y. Kim, G. Seong, C.H. Park, S. Kim, C.M. Doherty, A.W. Thornton, A.J. Hill, Tuning microcavities in thermally rearranged polymer

membranes for CO 2 capture w, (2012) 4365–4373. https://doi.org/10.1039/c2cp23729f.

[33] Q. Liu, D.R. Paul, B.D. Freeman, Gas permeation and mechanical properties of thermally rearranged (TR) copolyimides, Polymer (Guildf). (2016). https://doi.org/10.1016/j.polymer.2015.11.051.

[34] L.M. Robeson, The upper bound revisited, J. Memb. Sci. 320 (2008) 390–400. https://doi.org/10.1016/j.memsci.2008.04.030.

[35] T.T. Moore, W.J. Koros, Non-ideal effects in organic–inorganic materials for gas separation membranes, J. Mol. Struct. 739 (2005) 87–98. https://doi.org/10.1016/J.MOLSTRUC.2004.05.043.

[36] M. Galizia, W.S. Chi, Z.P. Smith, T.C. Merkel, R.W. Baker, B.D. Freeman, 50th Anniversary Perspective: Polymers and Mixed Matrix Membranes for Gas and Vapor Separation: A Review and Prospective Opportunities, Macromolecules. 50 (2017) 7809–7843. https://doi.org/10.1021/acs.macromol.7b01718.